Direct Seawater Electrolysis via Synergistic Acidification by Inorganic Precipitation and Proton Flux from Bipolar Membrane

Ji-Hyung Han[*a], Eunjin Jwa[a], Hongjun Lee[b], Eun Joong Kim[c], Joo-Youn Nam[a], Kyo Sik Hwang[a], Namjo Jeong[a], Jiyeon Choi[a], Hanki Kim[a], Youn-Cheul Jeung[a], Taek Dong Chung[*c]

[a]Jeju Global Research Center, Korea Institute of Energy Research, Haemajihaean-ro 200, Gujwa-eup, Jeju, 63357, Republic of Korea

[b]Department of Environmental Engineering, Chungbuk National University, Chungdae-ro 1, Seowon-gu, Cheongju, Chungbuk, 28644, Republic of Korea

[c]Department of Chemistry, Seoul National University, Seoul, 08826, Republic of Korea

* Corresponding author: jihyung0760@kier.re.kr, tdchung@snu.ac.kr

Key words: direct seawater electrolysis, inorganic precipitation, bipolar membrane, acidification of seawater, water dissociation, electrolyte engineering

Abstract

This report describes direct seawater electrolysis (DSE) wherein natural seawater is used as a catholyte without filtration or pretreatment; seawater is acidified to a pH of 2 while hydroxide ions are produced at the cathode by the hydrogen evolution reaction (HER). It results from the cooperative effect of hydroxide ions trapped through inorganic precipitation at the cathode and proton flux from water dissociation in a bipolar membrane (BPM; used as a separator). The acidification of the catholyte in the proposed BPM-DSE substantially mitigates cathode passivation, eliminates the requirement of additional processes for treatment of inorganic precipitates dispersed in the catholyte, and reduces the cathode potential (E_c) required for the HER to enable long-term DSE. The BPM in this system plays a critical role in maintaining the electrolyte concentration, suppressing the chlorine evolution reaction (ClER), and maximizing the oxygen evolution reaction. These findings are expected to suggest a breakthrough toward large-scale operation of DSE that successfully overcomes challenges such as energy consumption, inorganic precipitation, ClER, and corrosion.

1. Introduction

Hydrogen is an important energy carrier for the development and maintenance of a low-carbon economy through sustainable energy generation [1]. Considering the cost reduction for the production of renewable electricity, particularly from solar PV and wind, water electrolysis has gained more attention for its utilization in green hydrogen production. Water electrolysis typically requires ultra-purified water, either directly in a proton exchange membrane water electrolyzer [2] or the use of 20–30% KOH aqueous solution for alkaline water electrolyzers [3]. The production of high-purity water involves costly extensive water

purification/desalination processes as well as the associated investments for plantation, land, maintenance, and transportation. Therefore, when building industrial-scale electrolyzers in arid desert regions along ocean coastlines, where long-term hydrogen production costs are expected to be the lowest [4], high financial investment and high energy consumption associated with water sources become a bottleneck [5,6].

To this end, seawater—which accounts for 96.5% of the global water supply—can be used for electrolysis because it serves as an unlimited resource. However, direct seawater electrolysis (DSE) faces several fundamental and engineering challenges [5,6]. Corrosion due to chlorine gas and chloride ions limits the stability of the anode and cathode. For the anode, highly selective catalysts for the oxygen evolution reaction (OER: $2H_2O \rightarrow O_2 + 4H^+ + 4e^-$) are essential to minimize the competing chlorine evolution reaction (ClER: $2Cl^- \rightarrow Cl_2 + 2e^-$). Although neutral pH is desirable for seawater ($pH_{seawater}$ ~ 8), alkalinized seawater is required to ensure highly selective OER, because the standard potential difference between OER and ClER is the largest (~480 mV) under alkaline conditions [7]. Recent studies have shown that the alkaline design with $NiFeO_x$ enables more than 200 mA/cm^2 for OER [8,9]. In addition, non-noble metals at near-neutral pH have been investigated as catalysts for their high selectivity toward the hydrogen evolution reaction (HER: $2H_2O + 4e^- \rightarrow H_2 + 2OH^-$) in seawater [10-15], and DSE using such catalysts will be cost-effective as natural seawater can be directly used.

However, the formation of inorganic precipitates, such as magnesium hydroxide ($Mg(OH)_2$), is the most persistent problem for cathode operation in seawater, because the HER abruptly increases pH. The deposit formation results in the blockage of the active sites of the catalysts and high cell voltage. Lu et al. reported that inorganic scaling on the surface of the cathode decreases the current density by 50% [10]. When an ion exchange membrane (IEM) is

used as a separator for asymmetric electrolytes [9] or for the efficient separation of the gas product, the inorganic precipitates adhered to the surface of the IEM can hinder ionic flow, which increases internal resistance. Additionally, suspended precipitates in a bulk electrolyte can be detrimental to the flow of feed solution in a stack during upscaling because the channels are easily clogged by fine particles. Despite the significance of the inorganic fouling, few studies have addressed inorganic precipitation concerning DSE. Numerous studies have used pure NaCl solutions [9,16-18], strong buffered seawater [15,19-21], or alkalinized seawater [8] to avoid precipitation, which is merely a temporary expedient. Moreover, the additional use of chemicals, such as strong buffer and caustic potash, is likely to increase the carbon footprint during installation and raw chemical production [22,23], negating the advantages of DSE.

In this study, we controlled inorganic precipitation by acidification of natural seawater without the use of any additional chemicals by using a bipolar membrane (BPM) as a separator, consisting of a cation exchange layer (CEL) and an anion exchange layer (AEL). The application of reverse bias accelerates water dissociation (WD: $H_2O \rightarrow H^+ + OH^-$) at the interface wherein the direct contact between CEL and AEL occurs. The produced hydroxide ions and protons migrate from the corresponding layers in opposite directions [24]. BPM is generally applied to use acidic catholyte and basic anolytes by considering the WD direction [25-35]. WD occurring within the BPM is considerably favorable for retaining dissimilar catholytes and anolytes in electrolytes as well as for maintaining electrolyte concentration and pH during electrolysis, thus allowing a wide range of catalysts and electrolytes to be considered. In this respect, BPM under reverse bias suggests a considerable opportunity for DSE. Nevertheless, to the best of our knowledge, only a few studies on DSE have utilized real seawater as a catholyte. A combination of seawater and BPM was reported for CO_2 extraction in electrodialysis (ED), in which seawater was used as a feed solution rather than an electrolyte for the cathode [36].

Herein, we report DSE during which the catholyte (natural seawater) is acidified in the absence of additional physical or chemical processes. A BPM was employed as the separator to acidify seawater around the cathode by supplying protons from WD. Inorganic precipitation at the cathode surface captures hydroxide ions produced from the HER, thereby impeding pH rise. WD in the BPM and inorganic precipitation effectively acidify the natural seawater at the cathode to suppress the overpotential for the HER and the formation of dispersed inorganic deposits. Such cooperative acidification combined with the intrinsic functions of the BPM enables unprecedentedly stable and efficient DSE. Additionally, we discuss the potential scale-up of electrolyzers, which could operate by feeding low-grade water and related infrastructures.

2. Experimental

2.1. Direct seawater electrolyzer

We used a batch-type electrolyzer, consisting of two chambers (acryl, internal dimension: 5 × 5 × 5 cm^3) with a BPM (Astom, Corp. Japan) as a separator. Fe catalyst is used for enhancing WD in the BPM [37]. Each chamber contained 120 mL of electrolyte. Pt-coated Ti mesh electrodes were used as the cathode and anode, respectively, with a geometrical area of 7.065 cm^2. The distance between the electrode and the BPM was 1 mm using a silicon gasket (thickness, 1 mm). Assembly of the electrolyzer was conducted with a custom holder, which simultaneously applied pressure to the two chambers on both sides using a movable stainless steel plate; 0.1 M NaOH or 0.5 M NaOH was used as the anolyte. Diverse saline water solutions were used as the catholytes: 0.5 M NaCl (45.9 mS/cm, pH 7.2), sea salt solution as artificial seawater (50 mS/cm, pH 8.4), and natural seawater (32.1 mS/cm, pH 8.4). Wastewater and brine were taken from a wastewater treatment plant and a desalination plant through reverse

osmosis. These catholytes were directly applied to the electrolyzer without filtration or purification.

2.2. Electrochemical characterization

Electrochemical testing was performed using a potentiostat (ZIVE MP2C, WonaTech, Republic of Korea). During the measurement of E_{cell} in chronopotentiometry, E_c and E_a were monitored against an Ag/AgCl reference electrode by using an auxiliary connection. The E_m across the membrane was measured using two reference electrodes. The produced gas was collected in a gas bag (50 mL, Dalian Delin Gas Packing Co., Ltd, China) in each chamber during the constant current test for a certain period. Then, the gas bag was connected to a gas chromatograph (GC 2014, Shimadzu, Japan) to evaluate the gas component and the amount of hydrogen and oxygen. IC was performed using an ICS-1600 instrument (Thermo Fisher Scientific).

2.3. Physical and chemical characterization

Inorganic deposits were analyzed using field-emission scanning electron microscopy (FE-SEM; S-4800, Hitachi, Japan) coupled with quantitative energy-dispersive X-ray spectroscopy (EDX; XMAX 50, Horiba, Japan). X-ray diffraction (XRD) analysis was performed using a Smartlab system (Rigaku, Japan). The surface of the BPM was analyzed using X-ray photoelectron spectroscopy (XPS; K-alpha, Thermo VG Scientific, England).

2.4. Calculation of Faradaic efficiency

The Faradaic efficiency was calculated as experimental moles of hydrogen, and oxygen was divided by the theoretical value.

$$\text{Faradaic efficiency} = \frac{experimental\ moles}{theretical\ moles} \times 100$$

$$\text{Experimental moles} = V / V_0$$

where V is the measured volume and V_0 is 24.45 L— the gas volume of 1 mol at 1 atm and 298 K.

$$\text{Theoretical moles} = I \times t / n \times F$$

where *I* is the measured current, *t* is the collection time for gas, *n* is the stoichiometric number of electrons consumed in the electrode reaction (*n* = 2 for hydrogen production, *n* = 4 for oxygen production from water electrolysis), and *F* is the Faraday constant.

3. Results and Discussion

3.1. pH variation as a function of catholytes: 0.5 M NaCl and seawater

At a constant current density (1 mA cm^{-2}), we monitored pH variations using different types of catholytes (0.5 M NaCl, sea salt solution as an artificial seawater, and natural seawater) using a batch-type direct seawater electrolyzer (BPM-DSE; **Fig. 1a**) by using a BPM (Astom Corp. Japan) as the separator. Each chamber contains 120 mL of electrolyte, and a silicon gasket (thickness, 1 mm) maintains the distance between the electrode and the BPM. We used an asymmetric electrolyte system; 0.1 M NaOH was used as an anolyte to suppress ClER. The Pt-coated Ti meshes were used as the cathode and anode.

(a)

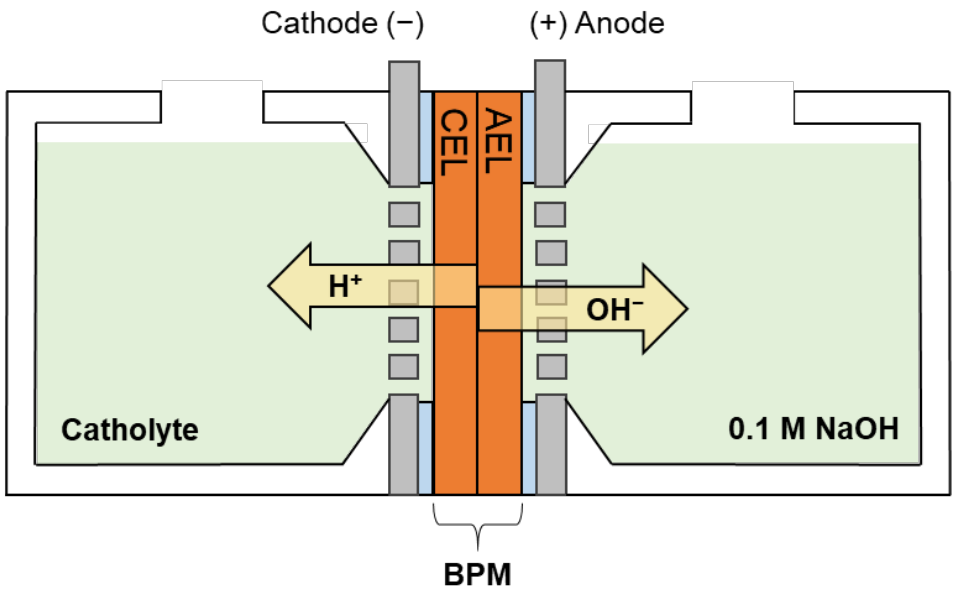
Cathode (−)
(+) Anode
CEL
AEL
H+
OH−
Catholyte
0.1 M NaOH
BPM

(b)

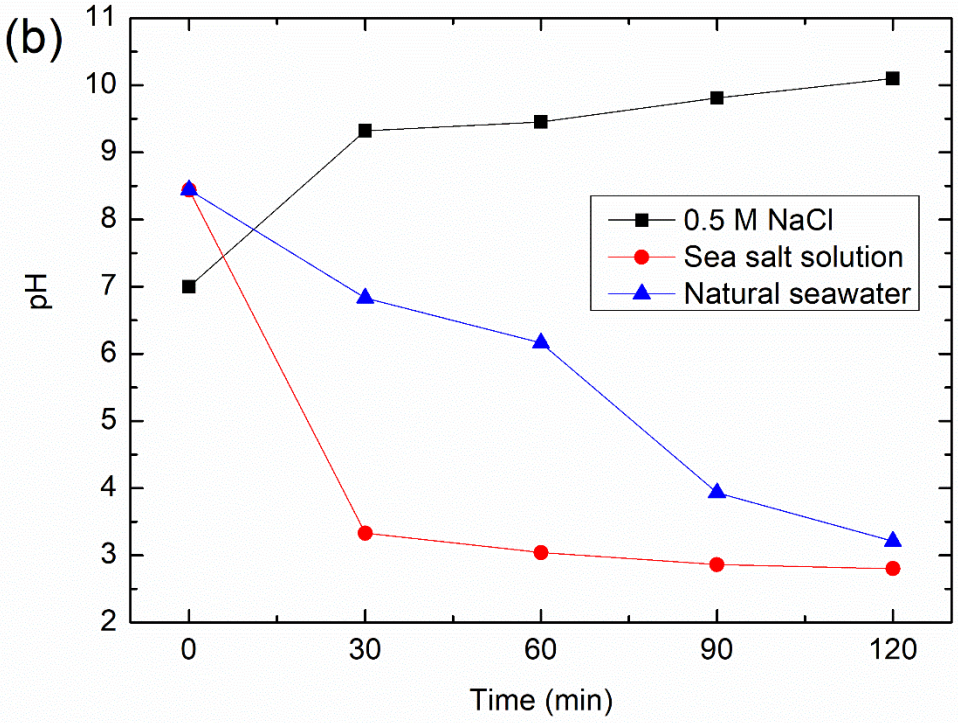
pH
Time (min)
0.5 M NaCl
Sea salt solution
Natural seawater
11
10
9
8
7
6
5
4
3
2
0
30
60
90
120

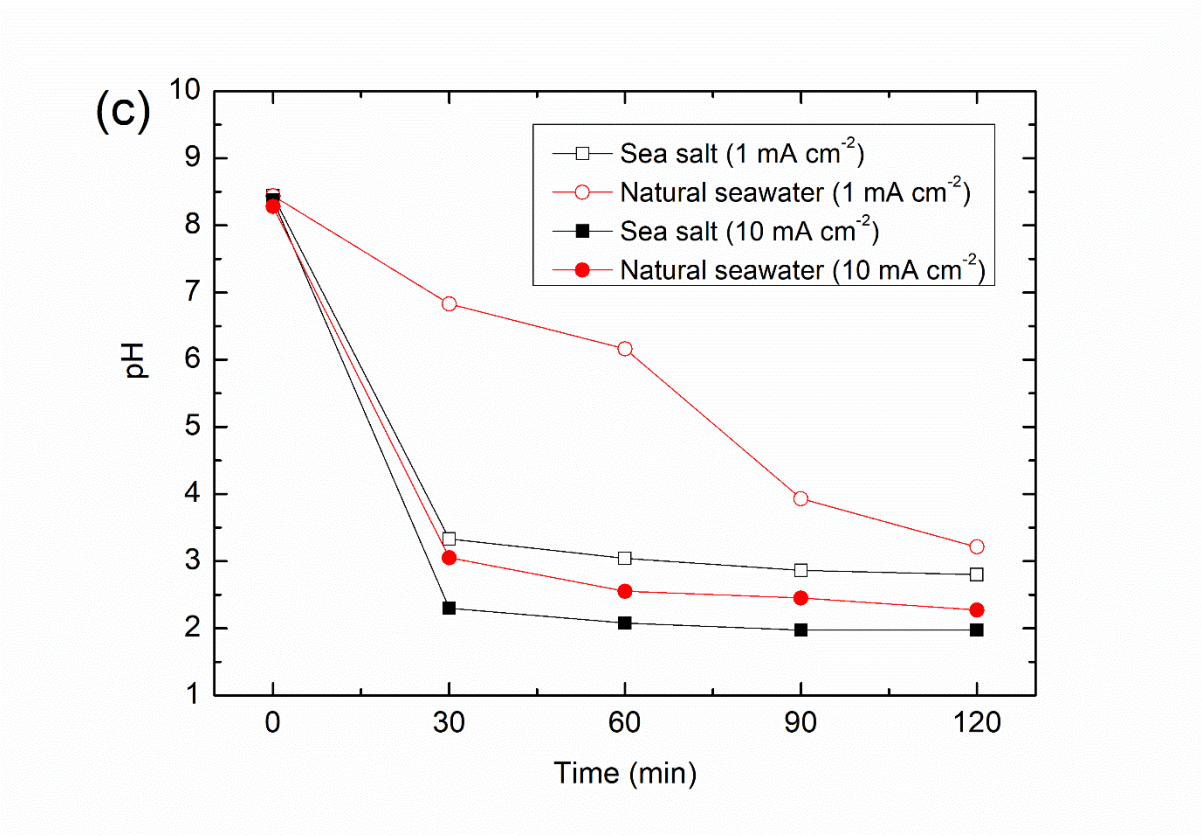

Figure 1. (a) Schematic of the BPM-DSE with an asymmetric electrolyte (catholyte // BPM // 0.1 M NaOH). The exposed area (7.065 cm^2) of the BPM with the electrolyte is the same with that of the electrodes. (b) pH variation over time with various catholytes (0.5 M NaCl, sea salt solution, and natural seawater). A current density of 1 mA cm^{-2} was applied to the electrolyzer for 2 h under reverse bias of the BPM. (c) pH variation over time with different current densities. (d) Photographs of the cathodes covered with inorganic precipitates.

Fig. 1b shows that the sea salt solution was acidified down to pH 3 in 30 min, whereas the pH of the 0.5 M NaCl solution increased to 10. Reminding of the fact that HER pushes pH up, we can see that the catholyte is exceedingly acidified. The pH of natural seawater slowly decreases, and the final pH is approximately 3 in 2 h. This is expected, as natural seawater contains a significant amount of various conjugate bases of polyprotic acids, including organic substances, which act as buffers. Its buffer capacity could matter much less at higher reaction rate. When the current density was 10 times higher (**Fig. 1c**), the pH of natural seawater decreased to 3 within 30 min. This trend works consistently over a wide range of current densities, but may cause a slower pH drop at much higher current densities (**Supporting information, Fig. S1**). Because the acidic pH of the catholyte results from a balance between the HER and the acidification at the cathode, we assume that the relative contribution of the HER to pH increases at 100 mA cm^{-2}.

Despite the acidification of the catholyte, the surface of the cathode was covered with inorganic precipitates (**Fig. 1d**). The HER makes the cathode surface basic even when the catholyte more or less apart from it is remarkably acidified. Multivalent ions at locally high pH readily form hydroxide salts, which are hardly soluble and deposited onto the cathode. In this case, the capture of free hydroxide ions by precipitation must be particularly considered, which indicates the availability of an additional acidification source for the solution. The organic substances in natural seawater appear to have a negligible effect on acidification, except for partial pH buffering.

3.2. Factors for acidification: $MgCl_2$ concentration and BPM arrangement

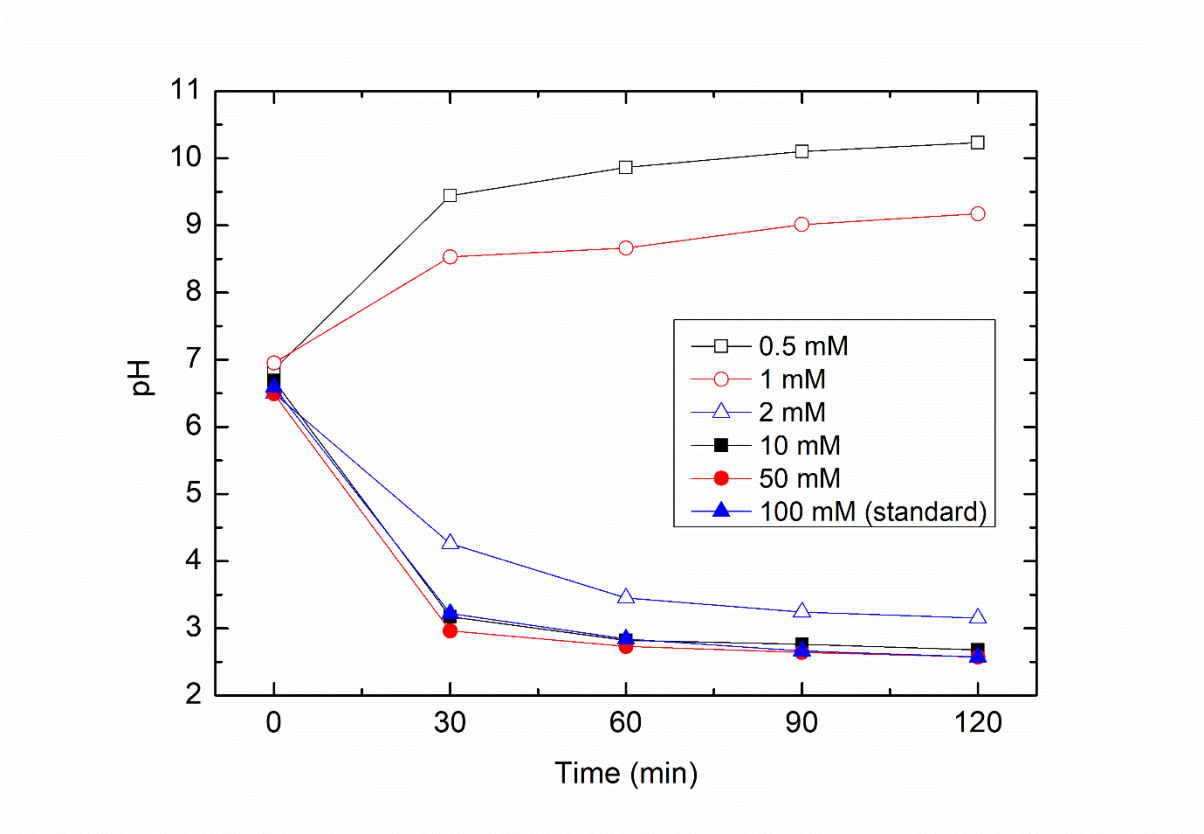

Figure 2. pH variation over time with various concentrations of $MgCl_2$ dissolved in 0.5 M NaCl as a catholyte at 1 mA cm^{-2} in the BPM-DSE (catholyte // BPM // 0.1 M NaOH).

The precipitates on the cathode resulting from seawater electrolysis are mostly magnesium hydroxide ($Mg(OH)_2$) with a very low solubility production constant (K_{sp} = 1.5×10^{-11}) (**Fig. S2**), whereas $Ca(OH)_2$ exists but has a considerably lower content because of the relatively high K_{sp} (5.5×10^{-6}). **Fig. 2** shows the effect of multivalent ions on pH variation as a function of magnesium chloride ($MgCl_2$) concentration. Although NaCl solution containing 1 mM $MgCl_2$ retains its alkalinity (~pH 10), $MgCl_2$ concentration of 2 mM or higher results in drastic acidification. As predicted, the study of the effect of $MgCl_2$ concentration on pH confirms that inorganic precipitation contributes to acidification of seawater by trapping hydroxide ions near the cathode to deter pH rise. Therefore, the presence of Mg^{2+} with the lowest K_{sp} among the six most abundant seawater ions (Cl^-, Na^+, SO_4^{2-}, Mg^{2+}, Ca^{2+}, and K^+) unexpectedly

contributes to acidification in this BPM-DSE system, which is not observed in conventional DSE.

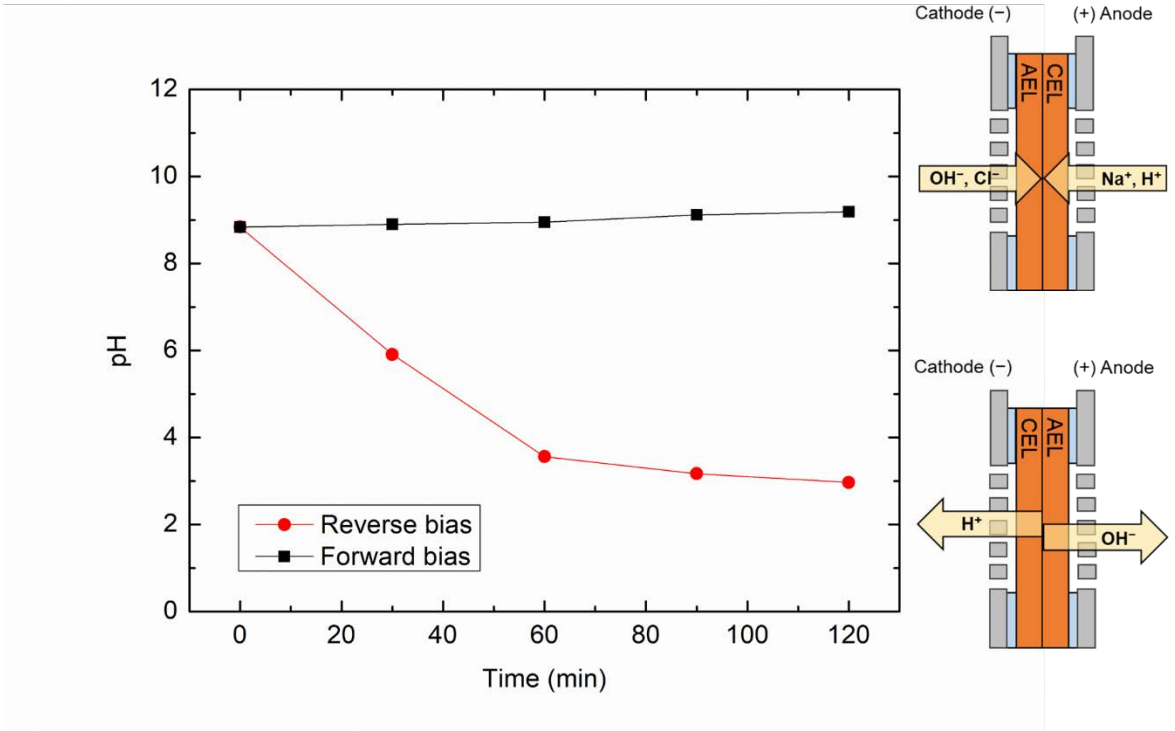

Figure 3. pH variation of the catholyte depending on arrangement of the BPM (forward vs. reverse) at 1 mA cm^{-2} in the BPM-DSE (sea salt solution // BPM // 0.1 M NaOH). AEL of the BPM facing toward the cathode corresponds to forward bias.

WD—a source of acidification in addition to presence of (primarily magnesium) hydroxide salts—occurs at the CEL/AEL interface in the BPM under reverse bias. The electric field across the interface—which contains catalysts such as polymers and metal oxides that promote WD [38,39]—continues producing and transporting protons and hydroxide ions through each permselective membrane in opposite directions. It produces continuous supply of protons and hydroxide ions into catholyte and anolyte, respectively.

Fig. 3 demonstrates the effect of proton flux on seawater acidification. Cations and anions in a BPM move in opposite directions under a unidirectional electric field. Upon forward bias, cations and anions gather at the CEL/AEL interface and pass through the BPM. Because only low resistance leads to a negligible potential drop across the BPM, no WD occurs. Therefore, the major charge carriers are Na^+ and Cl^-, rather than H^+ and OH^-. The sea salt solution never becomes acidic but maintains weak alkalinity (~ pH 9). In contrast, reverse bias makes the catholyte acidic, revealing that the protons produced from WD in the BPM under reverse bias are responsible for acidification. Consequently, we can identify two sources, hydroxide precipitation and WD, that can acidify the catholyte when the BPM is arranged to apply reverse bias.

3.3. Mechanism for acidification of seawater in BPM-DSE

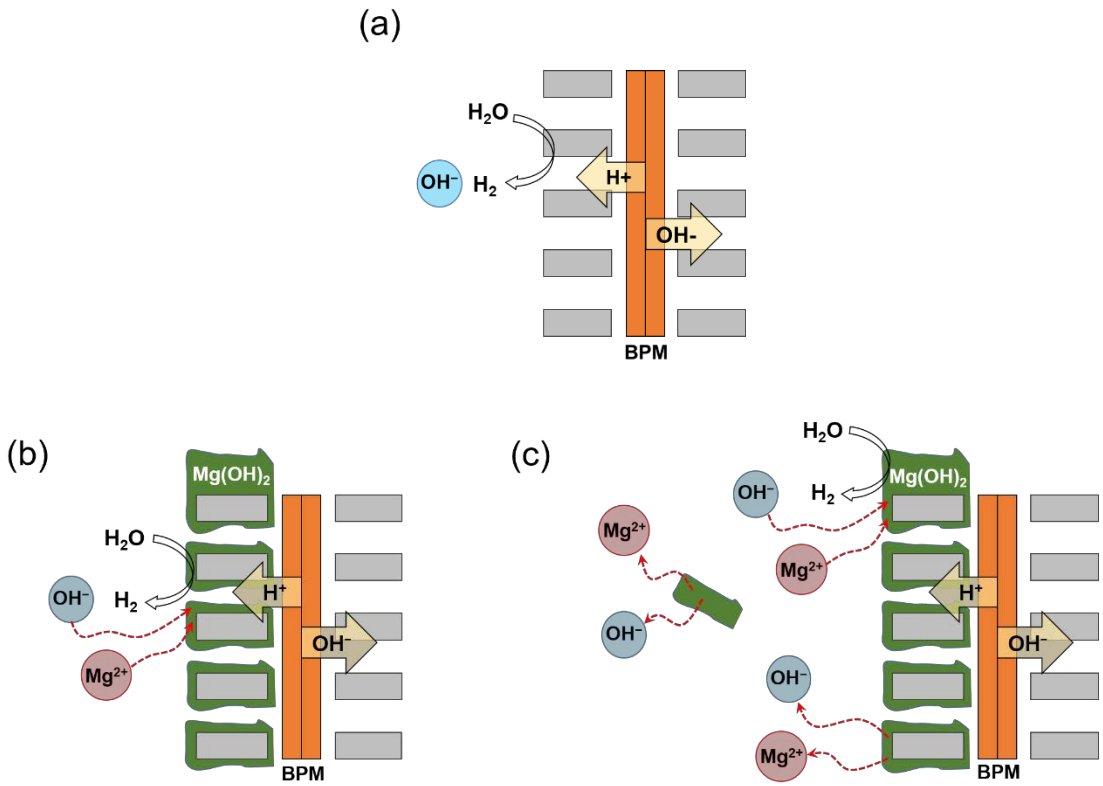

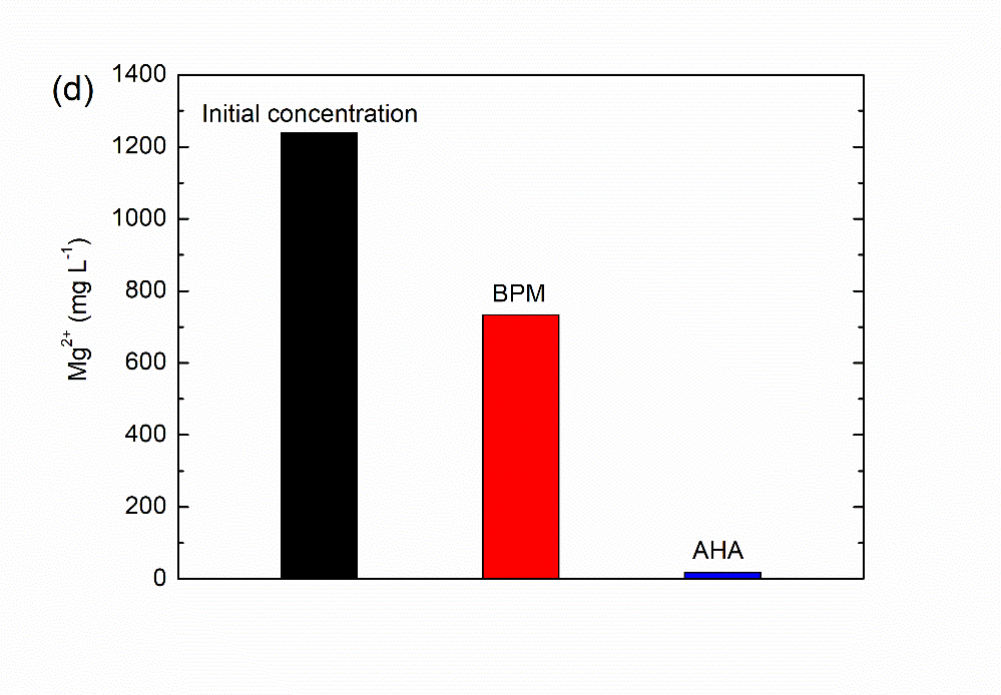

Figure 4. (a) Basification of NaCl solution without multivalent cations. (b) Initial and (c) final stages of seawater acidification. Inorganic precipitation and proton flux from WD in the BPM acidify the seawater as the catholyte. (d) Concentrations of Mg^{2+} ions in the sea salt solution determined after 100 h of operation at 10 mA cm^{-2} when using the BPM or AHA (an anion exchange membrane with high alkali resistance (Astom Corp., Japan)) as a separator.

The aforementioned experimental results help in determining a mechanism for the acidification of seawater in the BPM-DSE (**Fig. 4**). A high concentration of hydroxide ions (blue circles) generated from the HER causes the basification of the catholyte despite the proton supply from the WD in the BPM when a pure NaCl solution is used as a catholyte (**Fig. 4a**). On the other hand, abundant Mg^{2+} ions (red circles) are associated with hydroxide ions in seawater (**Fig. 4b**). Mg^{2+} ions capture hydroxide ions created by the HER to prevent the basification of the bulk catholyte. The BPM simultaneously provides protons that cooperate with hydroxide precipitation to acidify seawater.

Because the inorganic precipitates are likely to be soluble at low pH (**Fig. 4c**), the salt film is unlikely to become excessively thick; thus, resistance is controlled, indicating that additional acidification due to proton supply from the BPM helps maintain the appropriate thickness of the film. The Pt surface of the mesh cathode is partially exposed to the catholyte so that hydrogen evolution can break down the inorganic precipitates. This is confirmed by the inorganic debris of a mesh-shaped cathode floating around the catholyte during electrolysis. These precipitates slowly dissolve in acidified seawater, and multivalent ions (Mg^{2+} and Ca^{2+}) continue to participate in precipitation throughout electrolysis with sufficient seawater feed.

The concentrations of Mg^{2+} cations in the sea salt solution after 100 h of operation at 10 mA cm^{-2} was quantified by ion chromatography (IC) (**Fig. 4d**). The Mg^{2+} concentration decreased to 60% of the initial concentration in the BPM-DSE but remained substantially high. The Ca^{2+} concentration (730 mg/L) retained 80% of its initial value (**Fig. S3**). When AHA—an anion exchange membrane with high alkali resistance (Astom Corp., Japan)—was used as a separator instead of the BPM, the Mg^{2+} concentration dropped drastically to 18 mg/L (1% of the initial concentration), and 18% of the initial concentration of Ca^{2+} remained. AHA does not supply protons to the catholyte, which converts to a strong alkaline solution (~ pH 12).

3.4. Decrease in cathode potential for HER

The HER increases local pH at the cathode surface and shifts the equilibrium potential (E_{eq}) negatively following the Nerntian relationship [40,41] in the standard hydrogen electrode scale.

$$E_{eq} = -0.059 \times pH \quad (1)$$

The acidification of seawater holds up negative shift of E_{eq} as pH does not rise. Hence, so does the cathode potential (E_c) for HER in this system. **Fig. 5** shows the changes in E_c when 0.5 M NaCl or sea salt solution is used as the catholyte in the BPM-DSE (catholyte // BPM // 0.5 M NaOH).

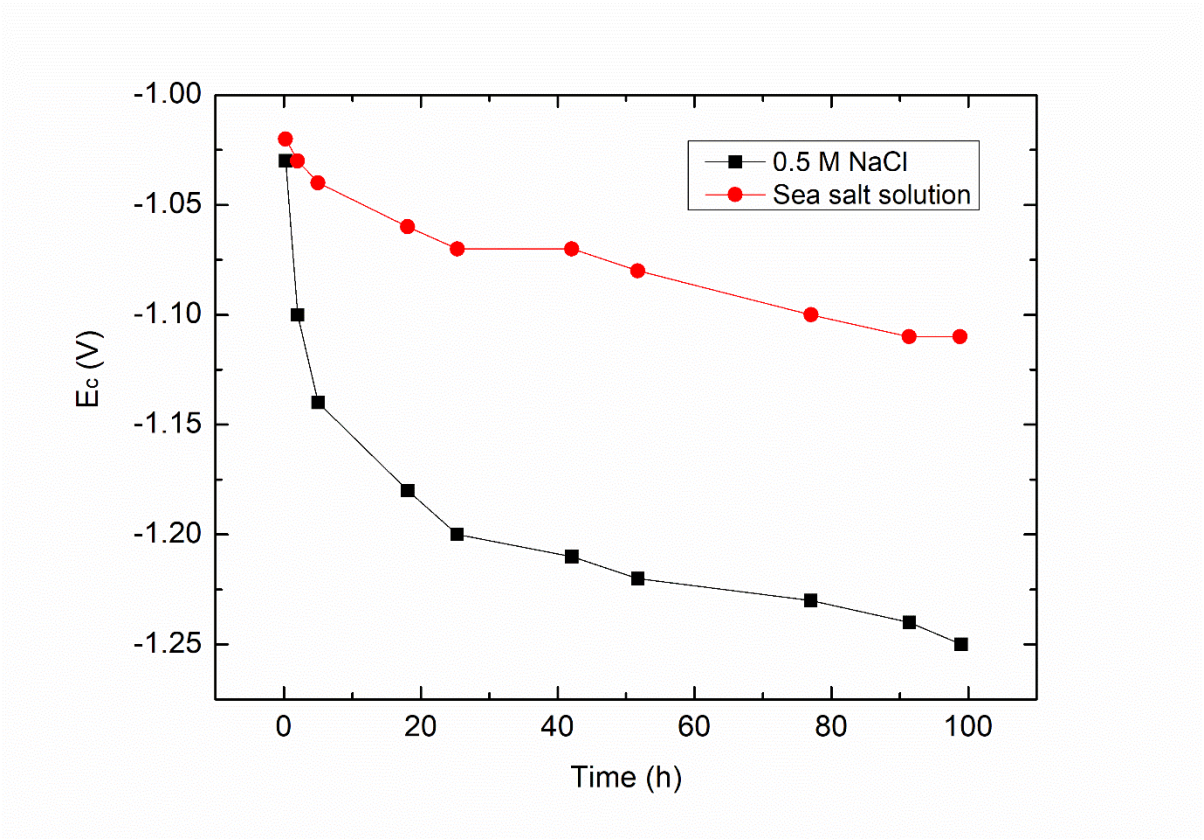

Figure 5. Shift of cathode potential (E_c) for two different catholytes (0.5 M NaCl or sea salt solution) at 10 mA cm^{-2}. E_c was recorded against an Ag/AgCl reference electrode (**Fig. S4**).

Although E_c starts at the same potential (~1 V), a steep negative shift appears when 0.5 M NaCl was used as the catholyte; the E_c of the sea salt solution shifts much more slowly. The large difference in the E_c slope at the beginning (~25 h) is caused by the alkalization of the NaCl solution and the acidification of seawater. The proton supply contribution from the BPM is the same for both catholytes and should be attributed to inorganic precipitation. Despite the high electrical resistance on the cathode surface due to the formation of a hydroxide salt film, acidification results in a less negative E_c of the sea salt solution than that of the NaCl solution. The acidification of the sea salt solution appropriately suppresses the growth of the film, which can eventually be dissolved, as described earlier. The difference in E_c (ΔE_c) is

constant at approximately 120–130 mV for operation longer than 100 h. Referring to the E_{eq} shift due to pH change, ΔE_c between 0.5 M NaCl and sea salt solution is thermodynamically estimated to be 590 mV—considerably higher than the measured value. This can be attributed to the larger overpotential for the HER due to cathode passivation by inorganic precipitates with low conductivity. Both cases showed a constant increase in E_{cell} over time, because the cathode is susceptible to corrosion due to the formation of Cl complexes [42,43]. The effect of corrosion on HER performance is considered to be dependent on the exposed area ratio of electrocatalysts to inorganic precipitates and the corrosion resistance of the electrocatalysts. Further investigation is needed to clarify the correlations between these factors.

3.5. Suppressed inorganic precipitation

The formation of dispersed inorganic precipitates is substantially suppressed in the proposed BPM-DSE system. Seawater in a cathode chamber with AHA becomes milky because of strong alkalinity (**Fig. 6a**), whereas the BPM-DSE maintains seawater transparency for more than 100 h as a result of acidification (**Fig. 6b**).

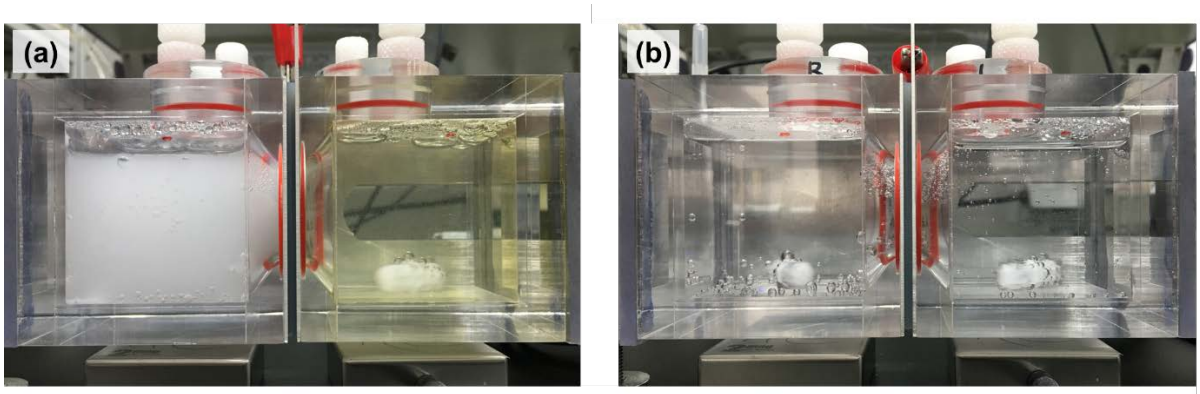

Figure 6. Photographs of electrolyzers (sea salt solution // membrane // 0.5 M NaOH) with AHA (a) or BPM (b) as a separator after 100 h operation at 10 mA cm^{-2}.

A large-scale water electrolyzer consists of many stacks of single cells and thin channels [44], which can be easily clogged by small particles, such as dispersed inorganic deposits. Seawater containing fewer precipitates during long-term electrolysis is significantly favorable for a stack system in which natural seawater is directly fed for use, eliminating the need to conduct a strong alkaline treatment and separation process for the removal of inorganic precipitates. This is an invaluable advantage for designing and constructing large-scale DSE systems, which need to be as compact and simple as possible. Consequently, seawater acidification is an effective electrolyte engineering strategy for DSE that facilitates reduced energy consumption and promotes sustainability.

3.6. Electrolyte concentration: BPM vs. CMB

The inherent properties of the BPM are crucial for the performance and stability of DSE based on acidification. In the asymmetric electrolyte system, the HER produces hydroxide ions in the catholyte, whereas hydroxide ions in the anolyte are consumed by the OER. As the operation continues, the concentration may become more polarized. The WD in the BPM can mitigate this in the proposed system. To demonstrate the functionality of the proposed BPM-DSE, we conducted long-term operations of DSE (sea salt solution // membrane // 0.5 M NaOH) with two types of membranes (BPM and CMB). The CMB (Astom Corp. Japan) is a cation exchange membrane with strong alkali resistance.

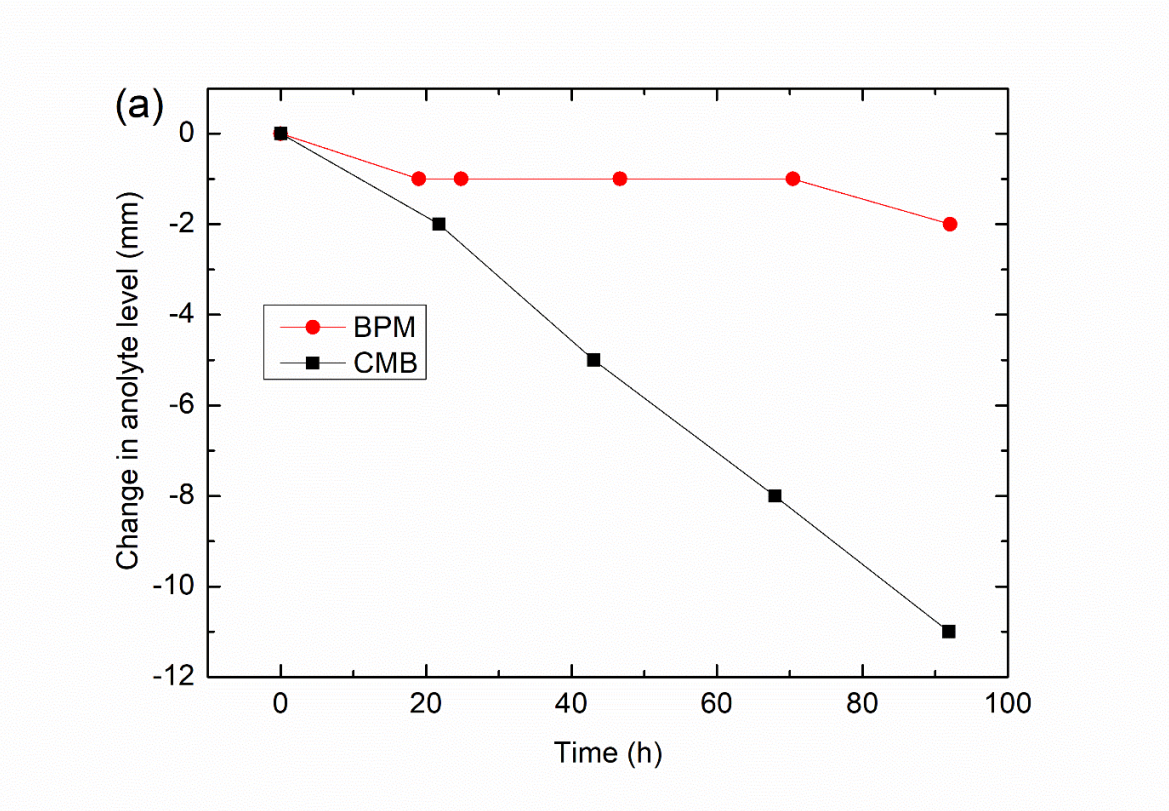
(a)
Change in anolyte level (mm)
0
-2
-4
-6
-8
-10
-12
BPM
CMB
0
20
40
60
80
100
Time (h)

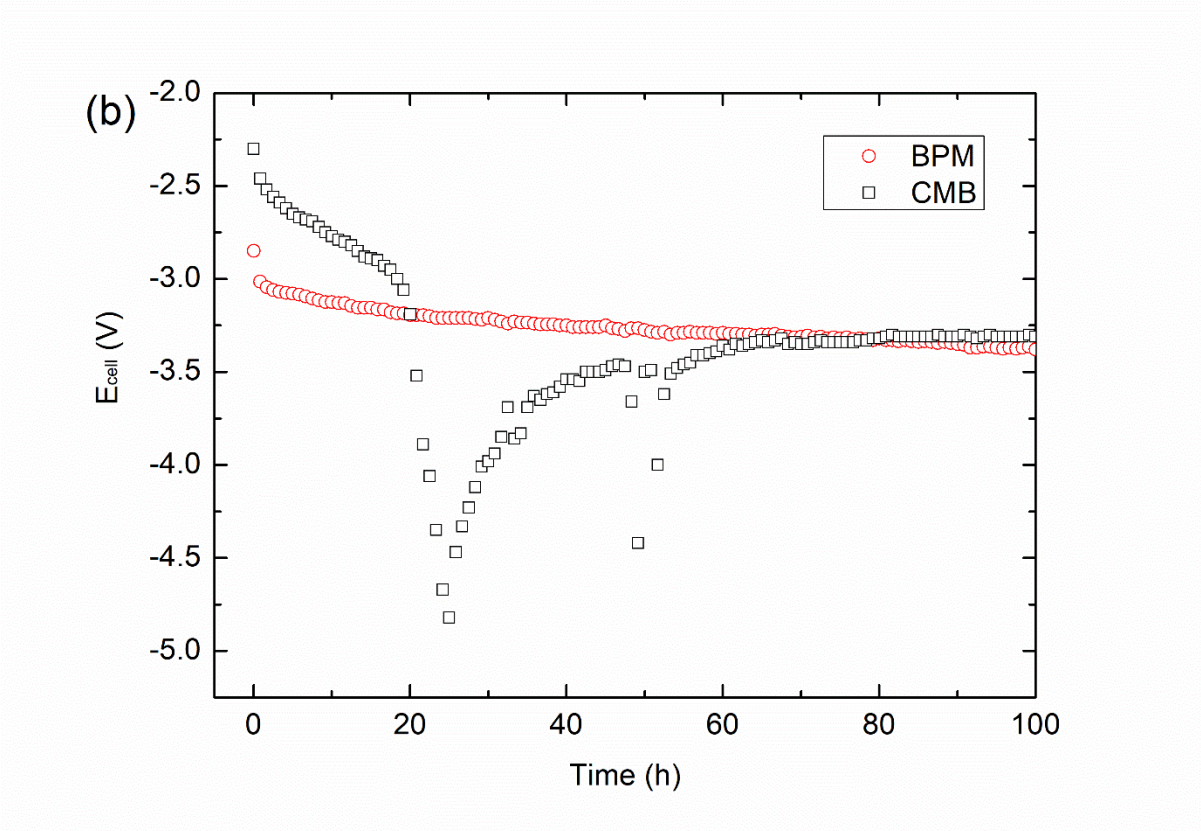
(b)
E_{cell} (V)
-2.0
-2.5
-3.0
-3.5
-4.0
-4.5
-5.0
BPM
CMB
0
20
40
60
80
100
Time (h)

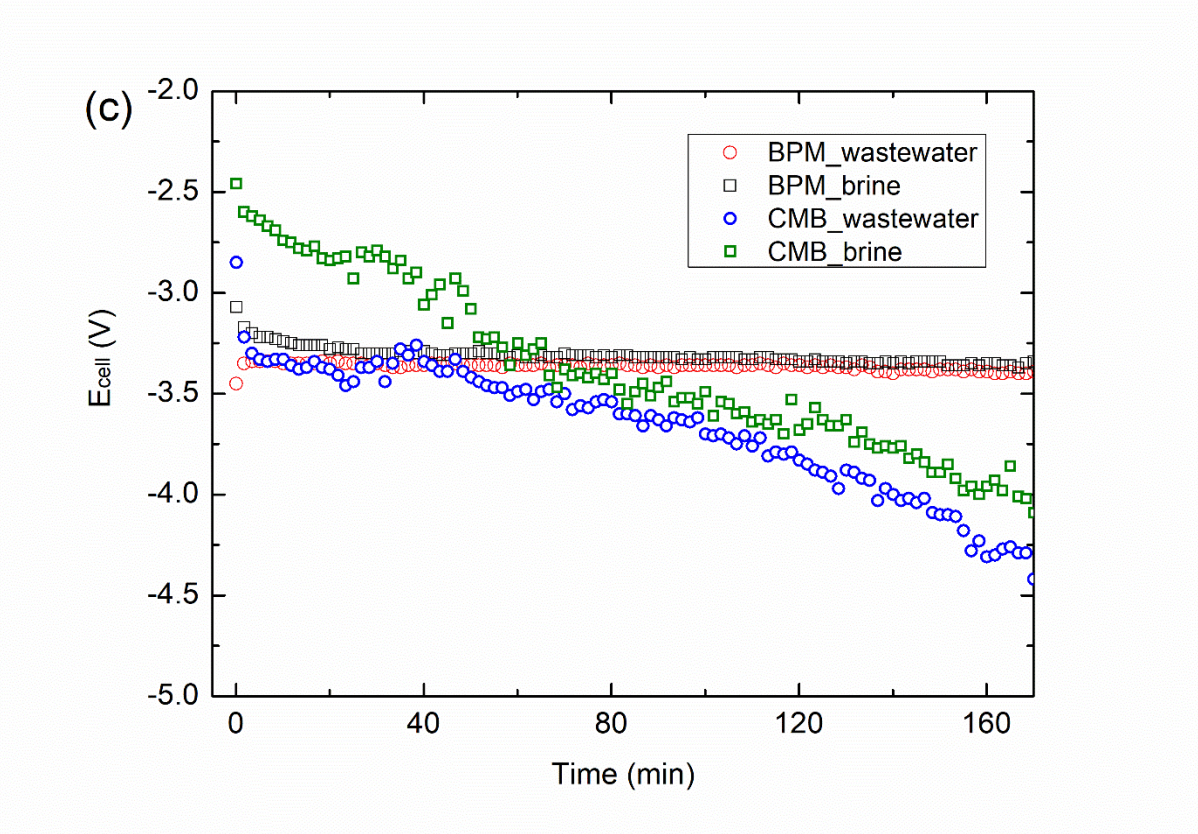

Figure 7. (a) Changes in the anolyte level as a function of time. Chronopotentiometric curves obtained with (b) BPM (or CMB)-DSE (sea salt solution // membrane // 0.5 M NaOH) at 10 mA cm^{-2} for 100 h and (c) BPM (or CMB)-DSE (catholyte // membrane // 0.1 M NaOH) fed with wastewater and brine as catholytes at 10 mA cm^{-2}.

Fig. 7a shows the change in electrolyte level depending on the membrane type. When using a CMB instead of a BPM, the anolyte level falls remarkably, exposing the electrode to the air changes (**Fig. S5**). Na^+ ions in the anolyte are transported to the catholyte to maintain charge neutrality, whereas anions are inhibited to cross over because of the charge selectivity of CMB (**Fig. S6a**). The reciprocal conductivities (**Fig. S6c**) show that the total electrolyte concentrations of the catholyte and anolyte continue to increase and decrease, respectively. Osmotic pressure develops commensurate with the height difference. An increasingly large difference in ion concentration between the anolyte and catholyte leads to a steep rise in E_m.

A short-term experiment with the CMB-DSE (0.5 M NaCl // CMB // 0.1 M NaOH) (**Fig. S6b**) revealed that the initial E_m (~200 mV) increased up to 2.5 V after 220 min, which increased E_{cell}; to maintain the high E_m, more electric energy consumption was required. In a long-term operation (**Fig. 7b**), the CMB also showed abrupt increase in E_{cell} up to -5 V at approximately 20 h. Therefore, cation exchange membranes, including CMBs, are unsuitable as separators for DSE with asymmetric electrolytes.

Contrarily, the electrolyte volumes and E_{cell} (in the case of the BPM) are almost constant, because WD in the BPM replenishes each electrolyte with protons and hydroxide ions. The ion supply in both directions maintains the electrolyte level and concentration, thereby stabilizing E_{cell}. Therefore, the BPM-DSE facilitates stable long-term operation of batch-type electrolyzer stacks without frequent electrolyte supplementation. This characteristic allows use of low-grade water with a variety of conductivities as water sources for hydrogen production. With wastewater (2.2 mS/cm, pH 7.9) and brine (85 mS/cm, pH 7.8) catholytes, E_{cell} and BPM-DSE operation are very stable (**Fig. 7c**). The pH of brine reaches 2 in 60 min, whereas that of wastewater is maintained at 8 in 2 h, because of the different degrees of inorganic precipitation (**Fig. S7**).

On the other hand, severe fluctuations (at approximately 50 h) appear with the CMB when a package for gas collection is connected to an electrolyzer adaptor, likely because of the sensitivity to gas flow, the reason for which remains unclear.

3.7. Effective disruption of Cl^- crossover and selective OER: BPM vs. AHA

In saline water electrolysis, Cl^- blockage is very important, because corrosion due to Cl complexes or chlorine gas has a considerable detrimental effect on the stability of electrocatalysts [5,45]. Continuous corrosion reduces the number of active sites of

electrocatalysts and increases cell voltage. Additionally, Cl_2 evolution and the formation of other active chlorine compounds require sophisticated infrastructure for their handling because of high corrosivity and toxicity. The BPM prevents Cl^- ions from crossing over to the anolyte; thus, the OER should occur selectively at the anode.

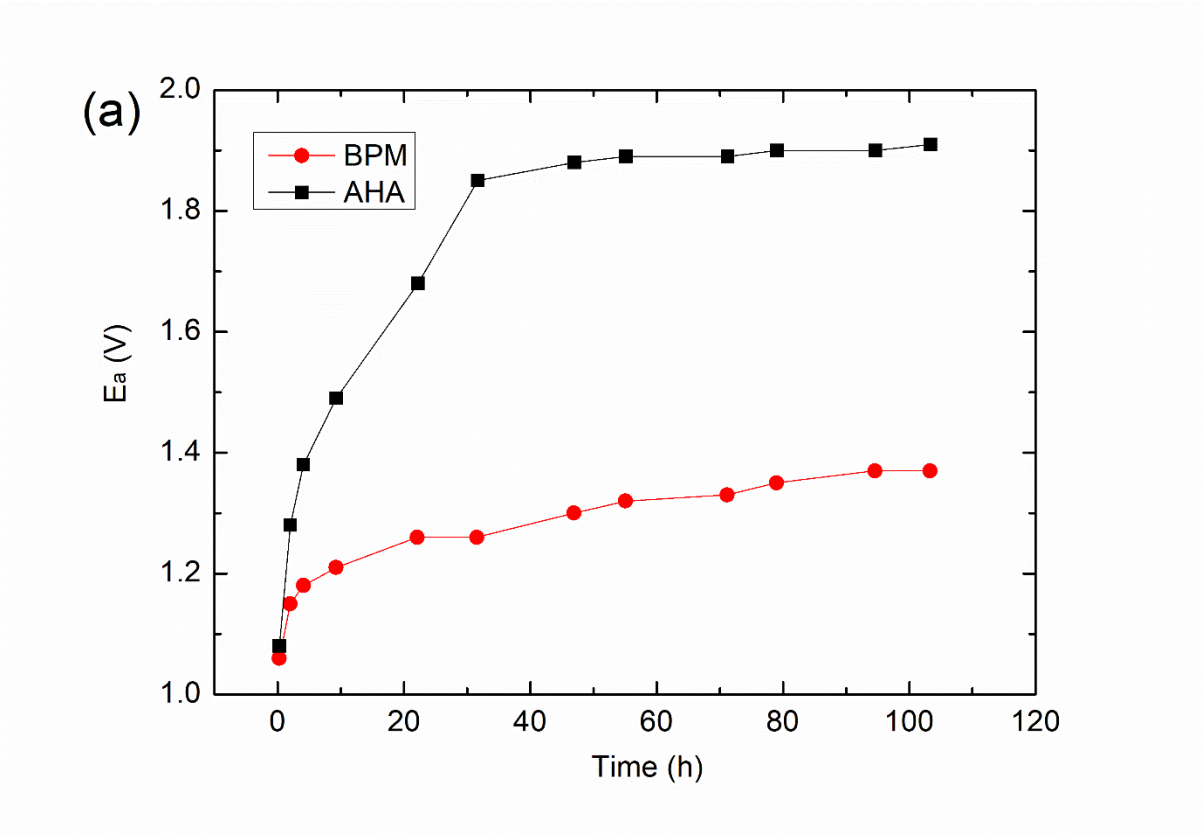

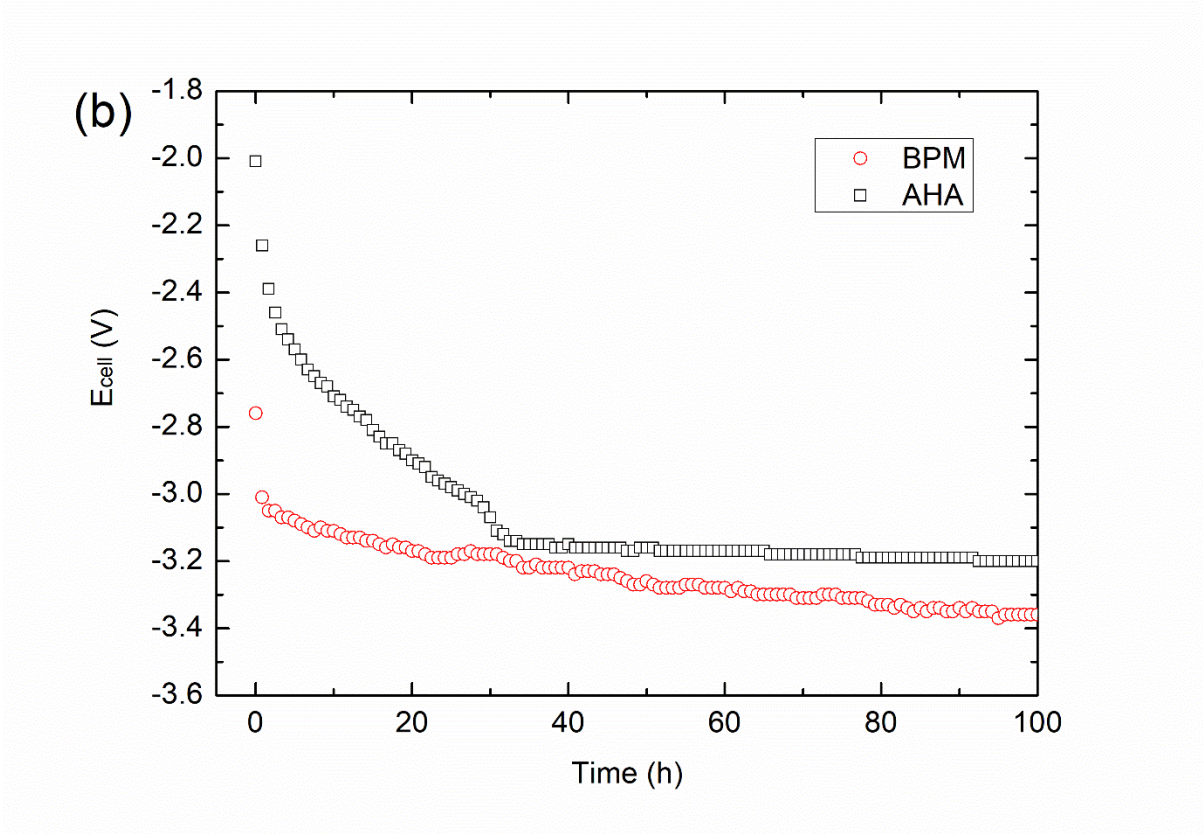

Figure 8. (a) Variation of anode potential (E_a) depending on membrane type at 10 mA cm^{-2} in the BPM (or AHA)-DSE (sea salt solution // membrane // 0.5 M NaOH). (b) chronopotentiometric curves of the BPM (or AHA)-DSE at 10 mA cm^{-2}.

Fig. 8a shows the variation of anode potential (E_a) when using the BPM and AHA as the separator during continuous operation for 100 h. The use of AHA causes a much larger increase in E_a than that of BPM, because of the high crossover of Cl^- ions into the anolyte due to anion permselectivity. We determined the concentrations of Cl^- ions in the anolyte through IC after 100 h of operation at 10 mA cm^{-2}. For the AHA, the Cl^- ion in the anolyte was 9679 mgL^{-1}—32 times higher than that for the BPM (301 mgL^{-1}). The Faradaic efficiency of O_2 production is very low (<16%), and the anolyte turns yellow (**Fig. 6a**). Approximately 500 mg/L of Cl^- ions appear to have been converted to Cl_2 gas through ClER, and a part of Cl_2 dissolves to form

hypochlorite (ClO^-). The anolyte becomes acidic, with its pH reduced to 5, as hydroxide ions are continuously consumed by the formation of hypochlorite ($Cl_2(g) + 2OH^- \rightarrow ClO^-(aq) + Cl^-(aq) + H_2O(aq)$) and concomitant OER. Such acidic conditions accelerate ClER, whereas the E_a of the BPM is much less positive than that of the AHA; the difference in E_a exceeds 500 mV. The Cl^- ion concentration at the anolyte–BPM interface is very low, indicating effective disruption of Cl^-crossover. Furthermore, through WD, the continuous supply of hydroxide ions is facilitated, which allows the retention of anolyte alkalinity. The resultant pH of the anolyte in the BPM-DSE is approximately 13, which is sufficiently high for the selective OER in the presence of Cl^- ions. Consequently, the BPM-DSE produced highly purified H_2 (99%) and O_2 (89%) with high Faradaic efficiency (96% for H_2, 85% for O_2), which was confirmed by GC measurements.

The consequent E_{cell} changes at over 100 h are shown in **Fig. 8b**. Because we apply reverse bias, the resistance of the BPM is much higher than that of the AHA. Therefore, the BPM is predicted to be unfavorable in terms of E_{cell}. The initial E_{cell} value of the BPM is approximately -2.76 V, which is more negative than that of the AHA (-2.01 V). The E_a of the AHA increases during the first 30 h (at a faster rate than that of the BPM, **Fig. 8a**). ΔE_{cell} at 100 h was decreased to ~160 mV. This is insignificant for the BPM-DSE in terms of energy consumption. E_c makes a minor contribution to the change in E_{cell} (**Fig. S8**). The E_c difference between the two electrolyzers is smaller than that observed in **Fig. 5**. Presumably thin inorganic deposits formed on the cathode in basified seawater blocks the diffusion of Cl^- ions to the electrode surface that suppresses corrosion. More studies need to be conducted to further investigate the correlation between inorganic deposits and corrosion in seawater.

Additionally, the proton flux from the WD in the BPM prevents inorganic scaling at the CEL of the BPM (**Fig. S9**). The AHA and CMB allow the disadvantageous formation of dense

precipitates on the side facing the cathode, hampering ionic flow across the membrane. In contrast, the BPM facilitates a lower extent of deposition, which imparts invariant internal resistance during long-term DSE.

3.8. Further improvement of BPM-DSE

Notwithstanding the effective acidification of seawater, E_{cell} for DSE is not sufficiently low and gradually increases during long-term operation. We suggest a few causes: chronic corrosion due to Cl complexes and overpotential for the WD in the BPM (**Fig. S10**), in which materials matter. Recently, a BPM in which WD occurs at very low overpotential (<10 mV at 20 mA cm^{-2}) was demonstrated [46,47]. The development of electrocatalysts for the HER and OER in seawater is also actively underway [8,9]. By applying the newly developed BPM and electrode materials, the performance and stability of the BPM-DSE can be significantly improved. There remain various parameters to simply tune, which might lead to appreciable improvement in practice, such as a ratio of electrolyte volume to electrode area, an area ratio of BPM to cathode, and so forth. Most of the aforementioned parameters are related to the acidification rate and thickness of inorganic precipitation. The optimal dimension and structure for the batch- or flow-typed stack of the BPM-DSE can be determined through simulation.

4. Conclusion

This is the first report showing that seawater as a catholyte is acidified to achieve a pH of 2 during DSE despite the significant generation of hydroxides in the HER. This is caused by the interaction between inorganic precipitation-induced trapping of hydroxide ions at the cathode surface and the proton supply from the WD in the BPM. The acidification of seawater reduces E_c and, thus, minimizes energy consumption, realizing DSE without the requirement of processes related to inorganic precipitate treatment. Additionally, because of intrinsic BPM

properties, the electrolyte crossover is effectively blocked, ClER is suppressed, and selectivity for OER is maximized. These advantages well exceed the energy loss due to WD. Therefore, the acidification of seawater with the BPM allows high-performance and stable DSE over long-term operation by overcoming critical problems of energy consumption, inorganic precipitation, ClER, and corrosion—a topic that has rarely advanced beyond the fundamental research. We hope that this work will stimulate the eco-friendly large-scale production of green hydrogen from direct seawater in arid desert regions by minimizing the carbon footprint during infrastructure and factory construction as well as during pre-/post treatment processes, such as water purification or desalination, production of raw chemicals (such as pure salt and sodium potash), and elimination of inorganic precipitates.

Author contributions

This study was designed, directed and coordinated by J.-H. Han as a primary author. T.D. Chung advised on scientific concept and writing the manuscript. H. Lee and E.J. Kim performed the electrochemical experiments. E. Jwa and J.-Y. Nam contributed to the IC experiments. K.S. Hwang and H. Kim participated in the design of electrolysis cell. N. Jeong and J. Choi contributed to the GC experiments. Y.-C. Jeung contributed to long-term data collection. All authors read and approved the final manuscript.

Conflicts of interest

There are no conflicts of interest to declare.

Acknowledgements

This work was conducted under the National Research Foundation of Korea (NRF) grant funded by the Korean government (MSIT) (No. 2019R1C1C1002847).

References

[1] G. Glenk, S. Reichelstein, Economics of converting renewable power to hydrogen, Nat. Energy 4 (2019) 216-222

[2] L. Ma, S. Sui, Y. Zhai, Investigations on high performance proton exchange membrane water electrolyzer, Int. J. Hydrog. Energy 34 (2009) 678-684

[3] K. Zeng, D. Zhang, Recent progress in alkaline water electrolysis for hydrogen production and applications, Prog. Energy Combust. Sci. 36 (2010) 307-326

[4] IEA, The Future of Hydrogen, Paris, https://www.iea.org/reports/the-future-of-hydrogen (2019)

[5] W. Tong, M. Forster, F. Dionigi, S. Dresp, R. Sadeghi Erami, P. Strasser, A. J. Cowan, P. Farràs, Electrolysis of low-grade and saline surface water, Nat. Energy 5 (2020) 367-377

[6] S. Dresp, F. Dionigi, M. Klingenhof, P. Strasser, Direct Electrolytic Splitting of Seawater: Opportunities and Challenges, ACS Energy Lett. 4 (2019) 933-942

[7] F. Dionigi, T. Reier, Z. Pawolek, M. Gliech, P. Strasser, Design Criteria, Operating Conditions, and Nickel–Iron Hydroxide Catalyst Materials for Selective Seawater Electrolysis, ChemSusChem 9 (2016) 962-972

[8] Y. Kuang, M. J. Kenney, Y. Meng, W.-H. Hung, Y. Liu, J. E. Huang, R. Prasanna, P. Li, Y. Li, L. Wang, M.-C. Lin, M. D. McGehee, X. Sun, H. Dai, Solar-driven, highly sustained splitting of seawater into hydrogen and oxygen fuels, Proc. Natl. Acad. Sci. U.S.A. 116 (2019) 6624-6629

[9] S. Dresp, T. Ngo Thanh, M. Klingenhof, S. Brückner, P. Hauke, P. Strasser, Efficient direct seawater electrolysers using selective alkaline NiFe-LDH as OER catalyst in asymmetric electrolyte feeds, Energy Environ. Sci. 13 (2020) 1725-1729

[10] X. Lu, J. Pan, E. Lovell, T. H. Tan, Y. H. Ng, R. Amal, A sea-change: manganese doped nickel/nickel oxide electrocatalysts for hydrogen generation from seawater, Energy Environ. Sci. 11 (2018) 1898-1910

[11] Y.-Y. Ma, C.-X. Wu, X.-J. Feng, H.-Q. Tan, L.-K. Yan, Y. Liu, Z.-H. Kang, E.-B. Wang, Y.-G. Li, Highly efficient hydrogen evolution from seawater by a low-cost and stable CoMoP@C electrocatalyst superior to Pt/C, Energy Environ. Sci. 10 (2017) 788-798

[12] H. Jin, X. Liu, A. Vasileff, Y. Jiao, Y. Zhao, Y. Zheng, S.-Z. Qiao, Single-Crystal Nitrogen-Rich Two-Dimensional Mo5N6 Nanosheets for Efficient and Stable Seawater Splitting, ACS Nano 12 (2018) 12761-12769

[13] Y. Zhao, Q. Tang, B. He, P. Yang, Carbide decorated carbon nanotube electrocatalyst for high-efficiency hydrogen evolution from seawater, RSC Adv. 6 (2016) 93267-93274

[14] J. Miao, F.-X. Xiao, H. B. Yang, S. Y. Khoo, J. Chen, Z. Fan, Y.-Y. Hsu, H. M. Chen, H. Zhang, B. Liu, Hierarchical Ni-Mo-S nanosheets on carbon fiber cloth: A flexible electrode for efficient hydrogen generation in neutral electrolyte, Sci. Adv. 1 (2015) e1500259

[15] S. Gao, G.-D. Li, Y. Liu, H. Chen, L.-L. Feng, Y. Wang, M. Yang, D. Wang, S. Wang, X. Zou, Electrocatalytic H2 production from seawater over Co, N-codoped nanocarbons, Nanoscale 7 (2015) 2306-2316

[16] S. Dresp, F. Dionigi, S. Loos, J. Ferreira de Araujo, C. Spöri, M. Gliech, H. Dau, P. Strasser, Direct Electrolytic Splitting of Seawater: Activity, Selectivity, Degradation, and Recovery Studied from the Molecular Catalyst Structure to the Electrolyzer Cell Level, Adv. Energy Mater. 8 (2018) 1800338

[17] B. C. M. Martindale, E. Reisner, Bi-Functional Iron-Only Electrodes for Efficient Water Splitting with Enhanced Stability through In Situ Electrochemical Regeneration, Adv. Energy Mater. 6 (2016) 1502095

[18] L. J. Song, H. M. Meng, Effect of carbon content on Ni–Fe–C electrodes for hydrogen evolution reaction in seawater, Int. J. Hydrogen Energy 35 (2010) 10060-10066

[19] S.-H. Hsu, J. Miao, L. Zhang, J. Gao, H. Wang, H. Tao, S.-F. Hung, A. Vasileff, S. Z. Qiao, B. Liu, An Earth-Abundant Catalyst-Based Seawater Photoelectrolysis System with 17.9% Solar-to-Hydrogen Efficiency, Adv. Mater. 30 (2018) 1707261

[20] Y. Zhao, B. Jin, Y. Zheng, H. Jin, Y. Jiao, S.-Z. Qiao, Charge State Manipulation of Cobalt Selenide Catalyst for Overall Seawater Electrolysis, Adv. Energy Mater. 8 (2018) 1801926

[21] Y. Zhao, B. Jin, A. Vasileff, Y. Jiao, S.-Z. Qiao, Interfacial nickel nitride/sulfide as a bifunctional electrode for highly efficient overall water/seawater electrolysis, J. Mater. Chem. A 7 (2019) 8117-8121

[22] H. Schultz, G. Bauer, E. Schachl, F. Hagedorn, P. Schmittinger. *Potassium Compounds*. (Wiley, 2000).

[23] J. Crook, A. Mousavi, The chlor-alkali process: A review of history and pollution, Environ. Forensics 17 (2016) 211-217

[24] T. Xu, Ion exchange membranes: State of their development and perspective, J. Memb. Sci. 263 (2005) 1-29

[25] X. Wang, R. Rossi, Z. Yan, W. Yang, M. A. Hickner, T. E. Mallouk, B. E. Logan, Balancing Water Dissociation and Current Densities To Enable Sustainable Hydrogen Production with Bipolar Membranes in Microbial Electrolysis Cells, Environ. Sci. Technol. 53 (2019) 14761-14768

[26] M. A. Blommaert, J. A. H. Verdonk, H. C. B. Blommaert, W. A. Smith, D. A. Vermaas, Reduced Ion Crossover in Bipolar Membrane Electrolysis via Increased Current Density, Molecular Size, and Valence, ACS Applied Energy Materials 3 (2020) 5804-5812

[27] H. Zhang, H. Wang, K. Jiao, J. Xuan, pH-differential design and operation of electrochemical and photoelectrochemical systems with bipolar membrane, Applied Energy 268 (2020) 115053

[28] S. Z. Oener, S. Ardo, S. W. Boettcher, Ionic Processes in Water Electrolysis: The Role of Ion-Selective Membranes, ACS Energy Lett. 2 (2017) 2625-2634

[29] D. A. Vermaas, M. Sassenburg, W. A. Smith, Photo-assisted water splitting with bipolar membrane induced pH gradients for practical solar fuel devices, J. Mater. Chem. A 3 (2015) 19556-19562

[30] K. Sun, R. Liu, Y. Chen, E. Verlage, N. S. Lewis, C. Xiang, A Stabilized, Intrinsically Safe, 10% Efficient, Solar-Driven Water-Splitting Cell Incorporating Earth-Abundant Electrocatalysts with Steady-State pH Gradients and Product Separation Enabled by a Bipolar Membrane, Adv. Energy Mater. 6 (2016) 1600379

[31] N. M. Vargas-Barbosa, G. M. Geise, M. A. Hickner, T. E. Mallouk, Assessing the Utility of Bipolar Membranes for use in Photoelectrochemical Water-Splitting Cells, ChemSusChem 7 (2014) 3017-3020

[32] K. Sakamaki, A. Watanabe, S. Usui, H. Matsuda, W. Sakashita, R. Kato, H. Endo, M. Sato, Photoelectrochemical visible light zero-bias hydrogen generation with membrane-based cells designed for decreasing overall water electrolysis voltage and water dissociation: the second stage, J. Appl. Electrochem. 49 (2019) 949-962

[33] J. Luo, D. A. Vermaas, D. Bi, A. Hagfeldt, W. A. Smith, M. Grätzel, Bipolar Membrane-Assisted Solar Water Splitting in Optimal pH, Adv. Energy Mater. 6 (2016) 1600100

[34] M. B. McDonald, S. Ardo, N. S. Lewis, M. S. Freund, Use of Bipolar Membranes for Maintaining Steady-State pH Gradients in Membrane-Supported, Solar-Driven Water Splitting, ChemSusChem 7 (2014) 3021-3027

[35] M. Ramdin, A. R. T. Morrison, M. de Groen, R. van Haperen, R. de Kler, E. Irtem, A. T. Laitinen, L. J. P. van den Broeke, T. Breugelmans, J. P. M. Trusler, W. d. Jong, T. J. H. Vlugt, High-Pressure Electrochemical Reduction of CO2 to Formic Acid/Formate: Effect of pH on the Downstream Separation Process and Economics, Ind. Eng. Chem. Res. 58 (2019) 22718-22740

[36] M. D. Eisaman, K. Parajuly, A. Tuganov, C. Eldershaw, N. Chang, K. A. Littau, CO2 extraction from seawater using bipolar membrane electrodialysis, Energy Environ. Sci. 5 (2012) 7346-7352

[37] F. Hanada, K. Hiraya, N. Ohmura, S. Tanaka. Bipolar membrane and method for its production. Japan patent EP0459820B1 (same as US 5221455, 1993) (1991).

[38] S. Mafé, P. Ramírez, A. Alcaraz, Electric field-assisted proton transfer and water dissociation at the junction of a fixed-charge bipolar membrane, Chem. Phys. Lett. 294 (1998) 406-412

[39] H. Strathmann, J. J. Krol, H. J. Rapp, G. Eigenberger, Limiting current density and water dissociation in bipolar membranes, J. Memb. Sci. 125 (1997) 123-142

[40] T. Shinagawa, K. Takanabe, Towards Versatile and Sustainable Hydrogen Production through Electrocatalytic Water Splitting: Electrolyte Engineering, ChemSusChem 10 (2017) 1318-1336

[41] J. E. Bennett, Electrodes for generation of hydrogen and oxygen from seawater, Int. J. Hydrogen Energy 5 (1980) 401-408

[42] A. Pavlišič, P. Jovanovič, V. S. Šelih, M. Šala, N. Hodnik, S. Hočevar, M. Gaberšček, The influence of chloride impurities on Pt/C fuel cell catalyst corrosion, ChemComm 50 (2014) 3732-3734

[43] K. Matsuoka, S. Sakamoto, K. Nakato, A. Hamada, Y. Itoh, Degradation of polymer electrolyte fuel cells under the existence of anion species, J. Power Sources 179 (2008) 560-565

[44] J. Hnat, R. Kodym, K. Denk, M. Paidar, J. Zitka, K. Bouzek, Design of a Zero-Gap Laboratory-Scale Polymer Electrolyte Membrane Alkaline Water Electrolysis Stack, Chem. Ing. Tech. 91 (2019) 821-832

[45] S. K. Sharma. *Green Corrosion Chemistry and Engineering: Opportunities and Challenges*. (Wiley, 2011).

[46] C. Shen, R. Wycisk, P. N. Pintauro, High performance electrospun bipolar membrane with a 3D junction, Energy Environ. Sci. 10 (2017) 1435-1442

[47] S. Z. Oener, M. J. Foster, S. W. Boettcher, Accelerating water dissociation in bipolar membranes and for electrocatalysis, Science 369 (2020) 1099-1103